Mirror-Image-Induced Magnetic Modes

Elisabet Xifré-Pérez,[†] Lei Shi,[‡,§] Umut Tuzer,[‡,§] Roberto Fenollosa,[‡,§] Fernando Ramiro-Manzano,[‡,§] Romain Quidant,[†,⊥] and Francisco Meseguer[‡,§,*]

[†]Institut de Ciencies Fotoniques (ICFO), Mediterranean Technology Park, 08860 Castelldefels, Barcelona, Spain, [‡]Centro de Tecnologías Físicas, Unidad Asociada ICMM/CSIC-UPV, Universidad Politécnica de Valencia, Av. Los Naranjos s/n, Valencia, 46022 Spain, [§]Instituto de Ciencia de Materiales de Madrid, CSIC, Madrid, 28049 Spain, and [⊥]Institució Catalana de Recerca i Estudis Avançats (ICREA), 08010 Barcelona, Spain

ABSTRACT Reflection in a mirror changes the handedness of the real world, and right-handed objects turn left-handed and vice versa (M. Gardner, *The Ambidextrous Universe*, Penguin Books, 1964). Also, we learn from electromagnetism textbooks that a flat metallic mirror transforms an electric charge into a virtual opposite charge. Consequently, the mirror image of a magnet is another parallel virtual magnet as the mirror image changes both the charge sign and the curl handedness. Here we report the dramatic modification in the optical response of a silicon nanocavity induced by the interaction with its image through a flat metallic mirror. The system of real and virtual dipoles can be interpreted as an effective magnetic dipole responsible for a strong enhancement of the cavity scattering cross section.

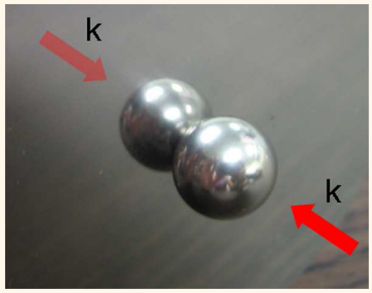

KEYWORDS: colloids · nanocavities · nanoparticles · charge image method · photonic interaction · metamaterials

It is well-known that the magnetic component of electromagnetic waves only plays a minor role in light−matter interaction.[1,2] However, the magnetic field plays a pivotal role in the optical response of metamaterials, with unique properties such as cloaking[3,4] and negative refraction.[5,6] A key ingredient of metamaterials is the existence of strong electric and/or magnetic resonances in the subwavelength scale. Metamaterials are customarily metallic because metals provide the restrictive conditions metamaterials need.[7] However, the property that makes metals good candidates for metamaterials (negative ε and eventually μ) is also responsible, because of the Kramers−Kronig relations, for large scattering and absorption losses, this being a restrictive bottleneck that limits their applicability.[8] Recently, several groups have proposed high refractive index nanostructures as alternative building blocks for metamaterials.[9−11] In particular, silicon colloids (SCs) feature well-defined low-order Mie resonances in the near-infrared (NIR)[10,12−15] and in the visible region[16,17] along with negative values of the electric and magnetic susceptibilities at optical frequencies.[18,19]

An essential step toward the assembly of a large number of SCs into metamaterials is to understand the optical interaction between two twin nanocavities. Unfortunately, the main drawback of the different methods for the fabrication of pure SCs reported so far[12,17,20,21] is the polydispersion of the dilutions, being challenging to find two colloids with exactly the same size. In analogy with the theory of image dipole in electrostatics, placing a nanocavity near a good conductor mirror[22] is a powerful alternative to achieve two interacting nanocavities with different polarizability.[22−24]

Here we experimentally demonstrate for the first time the mirror image interaction for dielectic nanocavities placed near a flat metallic mirror. The interaction between the nanocavity and its image results in a large amplification of the optical response of the particle at certain wavelength values. The mirror image effect transforms oscillating electrical dipoles into magnetic polarization currents, resulting in a large enhancement of the scattering cross section.

RESULTS AND DISCUSSION

The mirror image theory is a suitable method for solving the electric and magnetic field distributions of either a charge or a magnet near the flat surface of a perfect electric conductor (PEC).[1] For a charge near a PEC, the field distribution is obtained by replacing the PEC by a fictitious charge at the mirror image of the real charge but with opposite sign (Figure 1a). In the case of a magnet, the reflected mirror image has a magnetization vector parallel to the real one

* Address correspondence to fmese@fis.upv.es.

Received for review October 19, 2012 and accepted November 29, 2012.

Published online November 29, 2012
10.1021/nn304855t

© 2012 American Chemical Society

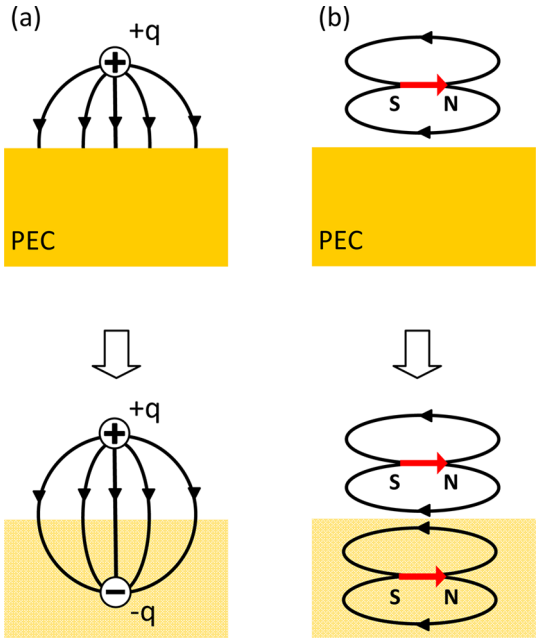

Figure 1. Schematic of the mirror image method for an electric charge (a) and a magnetic dipole (b).

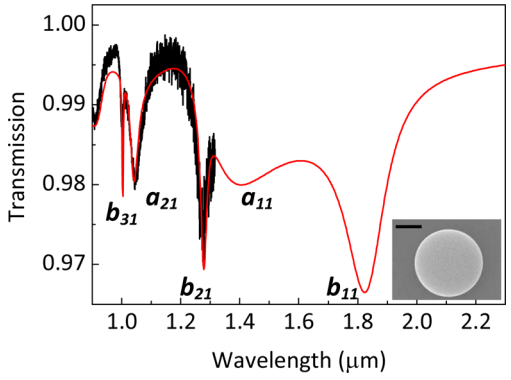

Figure 2. Transmission spectrum of a polycrystalline silicon sphere (d = 505 nm) on a glass substrate, experimental (black line) and simulated (red line). The labels indicate the order of the modes. Inset: SEM image of the silicon sphere. The scale bar is 200 nm.

(Figure 1b). The resonant modes of nanocavities can be envisaged as electric and magnetic oscillating multipoles strongly interacting with their mirror image counterparts. In this paper, we show that the method of the charge image can be extended to understand the modes of dielectric nanocavities placed near a flat metallic surface.

The smooth and regular spherical shape of SCs makes them very good nanocavities with high Q-factor optical resonances. Additionally, the high refractive index of Si allows well-defined low-order modes with spectral positions scaling with the colloid size.[25] In this study, we have used polycrystalline SCs[12] with diameters (d) between 500 and 750 nm, whose fundamental mode sits in the NIR range. Figure 2 shows a typical experimental transmission spectrum of one of these SCs lying on glass. A direct comparison with a

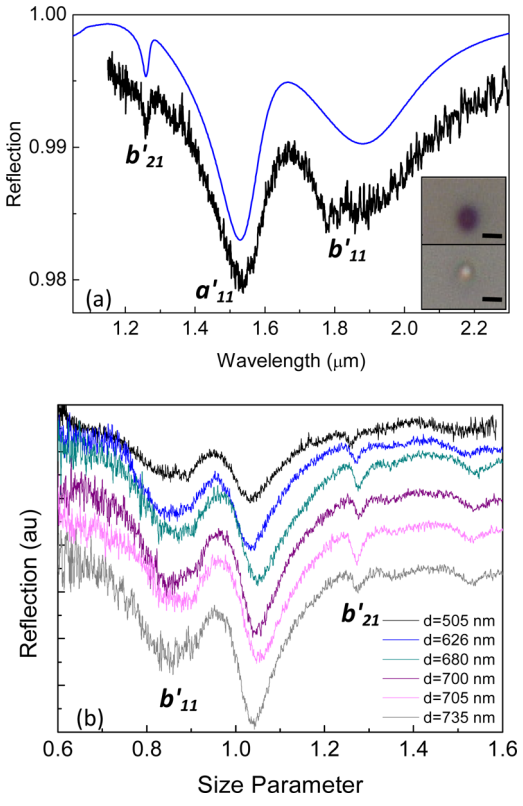

Figure 3. (a) Reflection spectrum of the 505 nm diameter sphere on a gold substrate measured with a FTIR (black line) and calculated with FDTD (blue line). The modes b'_{11}, a'_{11}, and b'_{21} are indicated. Inset: Optical microscope image with 1000× magnification of a silicon sphere placed on the gold substrate (top) and on the glass substrate (bottom). The scale bar is 1 μm. (b) Experimental reflection spectrum for different diameter silicon spheres placed on a gold substrate.

calculation based on the Mie theory[26,27] enables us to fully identify the different modes and precisely estimate the cavity diameter (d = 505 nm).

In order to study the influence of the mirror effect, the same SC nanocavity is transferred to a gold-coated substrate (30 μm thick) using micromanipulation techniques,[28] and the reflection spectrum is obtained (see Figure 3a). A first indication of the dramatic influence of the gold substrate comes from the change in the optical images of the cavity when transferred from one substrate to the other (inset of Figure 3). The apparent size of the particle on the gold substrate is much larger and with much higher contrast (top image) than on the glass plate (bottom image). Actually, our FTIR system failed to measure the spectrum of the cavity on glass because of the too weak signal.

When comparing the reflection spectrum of the colloid on gold (Figure 3a) with the spectrum of the SC on glass[29,30] (Figure 2), big differences are observed. The most important one concerns the appearance of a new and pronounced dip at around 1.53 μm (a'_{11}), much larger than other neighboring resonances at around 1.25 μm (b'_{21}) and 1.9 μm (b'_{11}). The optical

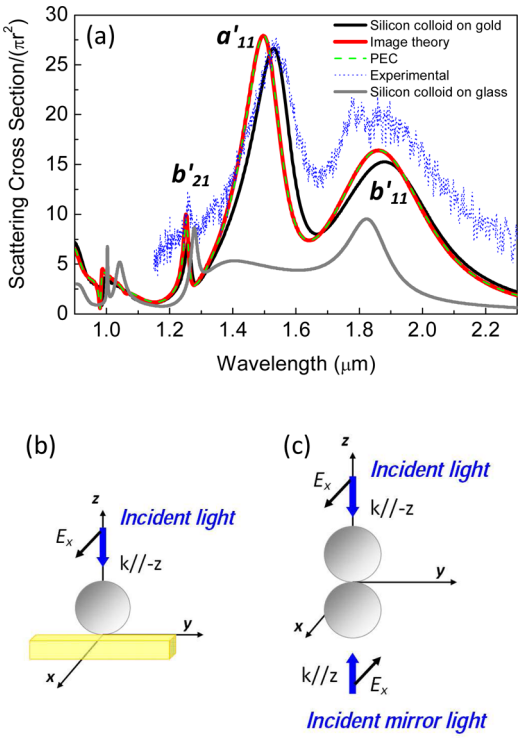

Figure 4. (a) Scattering cross section calculated for the 505 nm diameter silicon sphere on a gold surface (solid black), on a PEC (dashed green), and for two spheres—image theory—with d = 505 nm (solid red) and experimental cross section (dotted blue). The scattering cross section for the same colloid on glass is also plotted for comparison (solid gray). Schematic of the configuration for the cases: (b) sphere on gold substrate/PEC and (c) image theory.

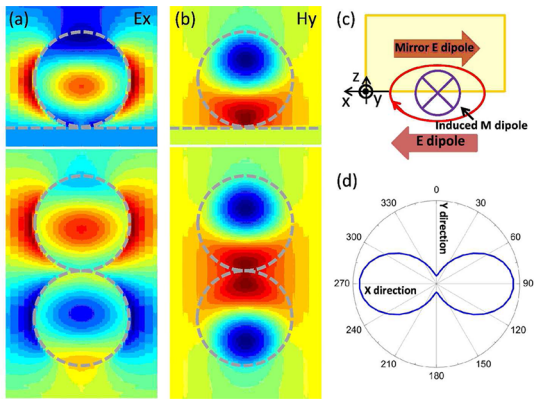

Figure 5. Ex field distribution (a) and Hy field distribution (b) in the x–z plane of the a'_{11} mode for the silicon colloid on a PEC model (top panels) and for the mirror image model (bottom panels). (c) Schematic figure of the magnetic dipole induced by the dipole and the mirror image dipole. (d) Scattering pattern of a'_{11} in the xy plane.

interaction of the nanocavity with its mirror image is *a priori* similar to that of two twin nanocavities in close contact. In the latter case, strong coupling between optical modes leads to splitting of each mode into a symmetric and antisymmetric hybridized mode.[31,32] However, in the mirror image case, due to the phase shift introduced by the metallic interface, such mode splitting is absent. Therefore, the mirror image interaction is antisymmetric for electric modes[22,24,33,34] and symmetric for the magnetic ones. Indeed, the interaction with the mirror image does not change the number of resonances. Instead, the a_{11} and b_{11} modes get red-shifted, from 1.41 to 1.53 μm and from 1.82 to 1.9 μm, respectively. A more striking effect though is the enhancement of the a'_{11} peak that becomes two times larger than the fundamental b'_{11}. All of these experimental observations are very well restituted by the modeled reflectivity obtained from the FDTD-calculated scattering cross section σ and the radius of the pinhole (r_p = 10 μm) used to limit the area containing the single colloid, by using $1 - \sigma/\pi r_p^2$. The small offset of the calculated data is attributed to the incertitude on the pinhole diameter.

To get further insight into the mirror image photonic interaction, we have measured the reflection spectrum of different size silicon nanocavities placed on a gold substrate. Figure 3b shows the evolution of the reflectivity spectrum with the size parameter x ($x = \pi d/\lambda$), where an offset between the spectra has been added for the sake of clarity. In all cases, the spectrum is dominated by the a'_{11} mode that always appears for a size parameter of about 1.04, with a scattering cross section value much larger than any other optical features. As expected, the spectrum is scaled with the sphere size, and the small variations in the position of the modes are due to the dispersion of the refractive index of silicon in the wavelength range analyzed.

At this stage, it is very instructive to compare the scattering cross section obtained for the nanocavity on gold with the one calculated for two other configurations: two touching SCs shined by two π-shift counter propagating laser beams depicted in Figure 4c (mirror image theory), and a SC on a perfect electric conductor (PEC)[22] (Figure 4b). In fact, the reflectivity properties of the gold surface are very similar to those of PEC (Supporting Information, Figure S1). In Figure 4a, we can see that all three configurations (black, red, and green-dashed lines for the SC on gold, the image theory, and the PEC configurations, respectively) show similar results and mimic very well the experimental data (dotted-blue line).

From a naïve perspective, one should expect that the presence of the mirror doubles the number of particles, so the scattering cross section would increase by a factor of 2, as observed for the magnetic modes b. However, the peak a'_{11} reaches scattering cross section values much beyond what this simple model shows. In order to understand the optical process behind such a result, we have calculated the field distribution of the a'_{11} peak. The E and H fields plotted in Figure 5a,b show that the metallic surface changes the nature of the modes. For example, the electric dipole mode (a_{11}) scatters much less light than the magnetic dipole mode (b_{11}). However, the existence of the mirror

induces an antisymmetric dipole image, resulting in an effective magnetic dipole mode,[24,33,34] with a high scattering cross section that dominates over any other mode of the nanocavity−mirror system. The origin of the induced magnetic dipole is similar to that appearing in metallic cut wire pairs.[24,35] However, in the present case, magnetic modes appear in the transparency region of silicon and thus benefit from much less absorption than those appearing for metallic nanostructures. In Figure 5a, the Ex field distribution of the a'_{11} mode for a single SC on the PEC model (top panel) and for the mirror image model (bottom panel) is shown. From the mirror image model, the antisymmetry between the electric dipole and mirror image electric dipole is clearly shown. The field distribution similarities for a'_{11} between the PEC case and the gold surface case are also shown in Figure S2 (Supporting Information). In contrast to the mirror image theory in electrostatics, two antisymmetric oscillating dipoles appear, inducing an effective magnetic dipole along the *y* direction (see Figure 5c), as shown by the scattering pattern of resonance a'_{11} in Figure 5d. The strong Hy field enhancement at the interface between the PEC and the SC is displayed in the scattering pattern of the mode (Figure 5d). The strongest scattering direction is parallel to the direction of the electric dipole but perpendicular to the induced magnetic dipole direction. Based on the principle of dipole radiation, this is a strong evidence of the magnetic dipole nature of a'_{11} mode.

CONCLUSIONS

To summarize, we have presented experimental evidence of the photonic interaction between a dielectric nanocavity and its image behind a mirror. We have shown that the scattering cross section of a silicon nanocavity is enhanced when located near a metallic mirror. Our analysis shows that the presence of the mirror turns the a_{11} electric mode into a magnetic-like mode, resulting in a huge enhancement of the scattering cross section.

MATERIALS AND METHODS

Silicon Colloids. In this work, we have used polycrystalline SCs with diameters between 500 and 750 nm. They were obtained by chemical vapor deposition techniques using disilane (Si_2H_6) as a precursor gas.[12,36] At high temperatures, disilane decomposes into solid silicon and hydrogen gas by the following chemical reaction: $Si_2H_6(g) \leftrightarrow 2Si(s) + 3H_2(g)$. We used a quartz tube (3 cm^2 in area and 15 cm long) as a reactor and introduced disilane gas at a pressure of 30 kPa. Part of the quartz tube was heated by a tubular oven at 400 °C for 30 min. This process produced amorphous silicon. An annealing treatment at 800 °C for 1 h in vacuum was used to convert amorphous to polycrystalline silicon.

Optical Characterizations. The transmission spectra were measured using a confocal homemade system. The SCs placed on glass substrate were illuminated with white nonpolarized light focused on the sample with a 20× long working distance Mitutoyo microscope objective. The transmitted light was collected with another twin microscope objective and sent to a beam expander coupled to an iHR320 Horiba Jobin Yvon spectrometer with an indium gallium arsenide (IGA) nitrogen refrigerated detector. The transmitted signal through the glass substrate (without the SC nanocavity) was taken as the reference signal. A pinhole was used to select the area of interest. The wavelength range measured with this confocal system goes from 0.9 to 1.3 μm.

The reflection spectra were measured using the homemade confocal system described for the transmission spectrum measures but using the same microscope objective for focusing and collecting the light reflected and a beam splitter. Due to the limited wavelength range of the IGA detector, the reflection spectra of the colloids placed on the gold mirror were also measured with a Bruker IF 66/S Fourier transform infrared (FTIR) spectrometer with a coupled microscope and a 15× Cassegrain objective (NA 0.4) for the wavelength range from 1.1 to 3 μm. The reflected signal from the gold surface (without the SC nanocavity) was taken as the reference signal. A pinhole of 20 μm diameter was used to select an area containing a single microsphere. The experimental cross section in Figure 4 has been obtained by the relation $\sigma = (1 - R)\pi r_p^2$.

Determination of the Colloidal Size. The diameter of the SC was precisely determined by calculating its transmittance spectrum with the Mie theory.[26,27] The silicon refractive index used for the calculation is a well-known wavelength-dependent value.[35] The calculated transmittance spectrum was fitted to the measured spectrum with only one fitting parameter, the colloidal size. With this method, a high precision of the SC diameter (with an error around 0.5%) was obtained.

Optical Simulations. The scattering cross section and the electric and magnetic field distributions for all of the structures were calculated with the commercial 3D Maxwell solver FDTD Solutions that employs the finite-difference time-domain (FDTD) method. The dielectric constants of gold and silicon have been taken from ref 37.

Conflict of Interest: The authors declare no competing financial interest.

Acknowledgment. L.S. thanks the MICINN (Estancias de profesores e investigadores extranjeros en centros españoles) fellowship program for the financial support. The authors acknowledge financial support from the following projects FIS2009-07812, Consolider 2007-0046 Nanolight, and the PROMETEO/2010/043.

Supporting Information Available: Figures S1, S2, and S3. This material is available free of charge *via* the Internet at http://pubs.acs.org.

REFERENCES AND NOTES

1. Jackson, J. D. *Classical Electrodynamics*; John Wiley & Sons: New York, 1962; pp 295−306.
2. Merlin, R. Metamaterials and the Landau−Lifshitz Permeability Argument: Large Permittivity Begets High-Frequency Magnetism. *Proc. Natl. Acad. Sci. U.S.A.* **2009**, *106*, 1693–1698.
3. Pendry, J. B.; Schurig, D.; Smith, D. R. Controlling Electromagnetic Fields. *Science* **2006**, *312*, 1780–1782.
4. Schurig, D.; Mock, J. J.; Justice, B. J.; Cummer, S. A.; Pendry, J. B.; Starr, A. F.; Smith, D. R. Metamaterial Electromagnetic Cloak at Microwave Frequencies. *Science* **2006**, *314*, 977–980.
5. Soukoulis, C. M.; Kafesaki, M.; Economou, E. N. Negative Index Materials: New Frontiers in Optics. *Adv. Mater.* **2006**, *18*, 1941–1952.
6. Hoffman, A. J.; Alekseyev, L.; Howard, S. S.; Franz, K. J.; Wasserman, D.; Podolskiy, V. A.; Narimanov, E. E.; Sivco, D. L.; Gmachl, C. Negative Refraction in Semiconductor Metamaterials. *Nat. Mater.* **2007**, *6*, 946–950.

7. Liu, N.; Mukherjee, S.; Bao, K.; Li, Y.; Brown, L. V.; Nordlander, P.; Halas, N. J. Manipulating Magnetic Plasmon Propagation in Metallic Nanocluster Networks. *ACS Nano* **2012**, *6*, 5482–5488.
8. Zheludev, N. I. The Road Ahead for Metamaterials. *Science* **2010**, *328*, 582–583.
9. Soukoulis, C. M.; Wegener, M. Past Achievements and Future Challenges in the Development of Three-Dimensional Photonic Metamaterials. *Nat. Photonics* **2011**, *5*, 523–530.
10. Shi, L.; Tuzer, T. U.; Fenollosa, R.; Meseguer, F. A New Dielectric Metamaterial Building Block with a Strong Magnetic Response below 1.5 Micrometers Region: Silicon Colloid Nanocavities. *Adv. Mater.* **2012**, *24*, 5934–5938.
11. Evlyukhin, A. B.; Reinhardt, C.; Seidel, A.; Luk'yanchuk, B. S.; Chichkov, B. N. Optical Response Features of Si-Nanoparticle Arrays. *Phys. Rev. B* **2010**, *82*, 045404.
12. Fenollosa, R.; Meseguer, F.; Tymczenko, M. Silicon Colloids: from Microcavities to Photonic Sponges. *Adv. Mater.* **2008**, *20*, 95–98.
13. Miroshnichenko, A. E.; Luk'yanchuk, B.; Maier, S. A.; Kivshar, Y. S. Optically Induced Interaction of Magnetic Moments in Hybrid Metamaterials. *ACS Nano* **2012**, *6*, 837–842.
14. Liu, W.; Miroshnichenko, A. E.; Neshev, D. N.; Kivshar, Y. S. Broadband Unidirectional Scattering by Magneto-Electric Core−Shell Nanoparticles. *ACS Nano* **2012**, *6*, 5489–5497.
15. Harris, J. T.; Hueso, J. L.; Korgel, B. A. Hydrogenated Amorphous Silicon (a-Si:H) Colloids. *Chem. Mater.* **2010**, *22*, 6378–6383.
16. Evlyukhin, A. B.; Novikov, S. M.; Zywietz, U.; Eriksen, R. L.; Reinhardt, C.; Bozhevolnyi, S. I.; Chichkov, B. N. Demonstration of Magnetic Dipole Resonances of Dielectric Nanospheres in the Visible Region. *Nano Lett.* **2012**, *12*, 3749–3755.
17. Kuznetsov, A. I.; Miroshnichenko, A. E.; Fu, Y. H.; Zhang, J.; Luk'yanchuk, B. Magnetic Light. *Sci. Rep.* **2012**, *2*, 492.
18. García-Etxarri, A.; Gómez-Medina, R.; Froufe-Pérez, L. S.; López, C.; Chantada, L.; Scheffold, F.; Aizpurua, J.; Nieto-Vesperinas, M.; Sáenz, J. J. Strong Magnetic Response of Submicron Silicon Particles in the Infrared. *Opt. Express* **2011**, *19*, 4815–4826.
19. Shi, L.; Meseguer, F. Magnetic Interaction in All Silicon Waveguide Spherical Coupler Device. *Opt. Express* **2012**, *20*, 22616–22626.
20. Li, X.; Pyatenko, A.; Shimizu, Y.; Wang, H.; Koga, K.; Koshizaki, N. Fabrication of Crystalline Silicon Spheres by Selective Laser Heating in Liquid Medium. *Langmuir* **2011**, *27*, 5076–5080.
21. Wu, J. J.; Nguyen, H. V.; Flagan, R. C. A Method for the Synthesis of Submicron Particles. *Langmuir* **1987**, *3*, 266–271.
22. Shi, L.; Xifré-Pérez, E.; Meseguer, F. Looking through the Mirror: Optical Microcavity-Mirror Image Photonic Interaction. *Opt. Express* **2012**, *20*, 11247–11255.
23. Lindell, I. V.; Alanen, E.; Mannersalo, K. Exact Image Method for Impedance Computation of Antennas above the Ground. *IEEE Trans. Antennas Propag.* **1985**, *33*, 937–945.
24. Liu, N.; Guo, H.; Fu, L.; Kaiser, S.; Schweizer, H.; Giessen, H. Plasmon Hybridization in Stacked Cut-Wire Metamaterials. *Adv. Mater.* **2007**, *19*, 3628–3632.
25. Xifré-Pérez, E.; Fenollosa, R.; Meseguer, F. Low Order Modes in Microcavities Based on Silicon Colloids. *Opt. Express* **2011**, *19*, 3455–3463.
26. Bohren, C. F.; Huffman, D. R. *Absorption and Scattering of Light by Small Particles*; John Wiley & Sons: New York, 1998: pp 82−129.
27. Barber, P. W.; and Hill, S. C. *Light Scattering by Particles: Computational Methods*; World Scientific: Singapore, 1990; pp 187−252.
28. Xifré-Pérez, E.; Domenech, J. D.; Fenollosa, R.; Muñoz, P.; Capmany, J.; Meseguer, F. All Silicon Waveguide Spherical Microcavity Coupler Device. *Opt. Express* **2011**, *19*, 3185–3192.
29. Bobbert, P. A.; Vlieger, J.; Greef, R. Light Reflection from a Substrate Sparsely Seeded with Spheres—Comparison with an Ellipsometric Experiment. *Phys. A* **1986**, *137*, 243–257.
30. Bobbert, P. A.; Vlieger, J. Light Scattering by a Sphere on a Substrate. *Phys. A* **1986**, *137*, 209–242.
31. Xifré-Pérez, E.; García de Abajo, F. J.; Fenollosa, R.; Meseguer, F. Photonic Binding in Silicon-Colloid Microcavities. *Phys. Rev. Lett.* **2009**, *103*, 103902.
32. García de Abajo, F. J. Interaction of Radiation and Fast Electrons with Clusters of Dielectrics: A Multiple Scattering Approach. *Phys. Rev. Lett.* **1999**, *82*, 2776–2779.
33. Albooyeh, M.; Simovski, C. R. Huge Local Field Enhancement in Perfect Plasmonic Absorbers. *Opt. Express* **2012**, *20*, 21888–21895.
34. Albooyeh, M.; Morits, D.; Simovski, C. R. Electromagnetic Characterization of Substrated Metasurfaces. *Metamaterials* **2011**, *5*, 178–205.
35. Shalaev, V. M.; Cai, W.; Chettiar, U. K.; Yuan, H.-K.; Sarychev, A. K.; Drachev, V. P.; Kildishev, A. V. Negative Index of Refraction in Optical Metamaterials. *Opt. Lett.* **2005**, *30*, 3356–3358.
36. O'Mara, W.; Herring, R. B.; Hunt, L. P. *Handbook of Semiconductor Silicon Technology*; Noyes Publications: Park Ridge, NJ, 1990; pp 7−9.
37. Palik, E. D. *Handbook of Optical Constants of Solids*; Academic Press: San Diego, CA, 1985; Vol. 1, pp 564−566.